RESEARCH ACTIVITIES

Photo-Molecular Science

Molecules respond to photon irradiation in a variety of ways, including photo-induced transitions and photochemical reactions. We have employed various light sources and experimental schemes to elucidate molecular structures and properties, and to control chemical reactions and molecular functions. We have also developed novel and advanced light sources for molecular science. Two of research facilities, the Laser Research Center for Molecular Science and the UVSOR Facility, conduct collaborative researches having intimate contacts with the Department of Photo-Molecular Science.

The main topics pursued in the Department include: Development of novel laser spectroscopic methods to reveal fundamental properties of molecules, development of high-resolution optical microscopic methods and application to nanomaterials, coherent control of molecules with ultrafast techniques, spectroscopy of inner-shell excited molecules and fundamental vacuum-UV photochemistry, investigation of the functionality of solid-state materials, developments of novel laser and synchrotron-orbit radiation sources, and so on.

Development of Advanced Near-Field Spectroscopy and Application to Nanometric Systems

Department of Photo-Molecular Science
Division of Photo-Molecular Science I

OKAMOTO, Hiromi	Professor
IMURA, Kohei	Assistant Professor
NARUSHIMA, Tetsuya	Assistant Professor
JIANG, Yuqiang	Post-Doctoral Fellow
HARADA, Yosuke	Post-Doctoral Fellow
WU, Huijun	Graduate Student
KIM, Su Il	Graduate Student*
NOMURA, Emiko	Secretary

There is much demand for the study of local optical properties of molecular assemblies and materials, to understand mesoscopic phenomena and/or to construct optoelectronic devices in the nanometric scale. Scanning near-field optical microscopy (SNOM), which enables spatial resolution beyond the diffraction limit of light, has been remarkably progressed in technology in the past decade. Combination of this advanced optical technology with various nonlinear and ultrafast laser spectroscopic methods may offer a direct probe of molecular dynamical processes in mesoscopic materials systems. It may provide essential and basic knowledge for analyzing origins of characteristic features and functionalities of the mesoscopic systems. We have constructed apparatuses for near-field dynamic spectroscopy with the femtosecond time resolution and the nanometer spatial resolution. They are capable of measuring conventional near-field transmission, emission, and Raman-scattering, and unique near-field two-photon induced emission and ultrafast transient transmission as well. Based on these methods, we are observing the characteristic spatio-temporal behavior of various metal nanoparticle systems and molecular assemblies, for the purpose of understanding nano-optical characteristics, spatial coherence of excitations, dynamics, *etc*. We also investigate the basic characteristics of near-field microscopic measurements.

1. Visualization of Plasmon Wavefunctions Induced in Various Metal Nanoparticles

We recently reported that wavefunctions of localized plasmon resonances of metal nanoparticles can be visualized by near-field transmission or two-photon excitation measurements.[1] The plasmons we visualized include the longitudinal modes of chemically synthesized gold and silver nanorods and in-plane modes of chemically synthesized gold triangular nanoplates. Figure 1 shows typical examples of near-field transmission images for longitudinal plasmon modes on a nanorod (the images correspond to the square moduli of the wavefunctions). We reported that the images show excellent agreement with calculated images of local density of electromagnetic states (LDOS) which correspond to the square moduli of the resonant plasmon wavefunctions.

We are extending the study to the metal nanostructures manufactured by the electron-beam lithography technique, in collaboration with researchers of other institution. We have obtained preliminary results for some metal nanostructures and have found characteristic plasmon waves. Such a study is essential as a basis to design unique optical properties and functions of metal nanostructures.

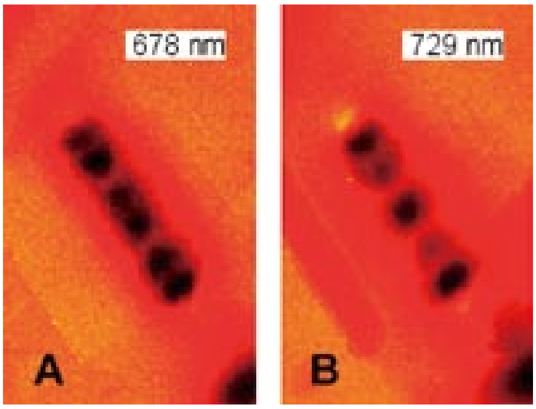

Figure 1. Near-field transmission images of a gold nanorod (diameter 20 nm, length 510 nm), observed at 678 nm (A) and 729 nm (B).

2. Ultrafast Transient Images of Gold Nanoparticles

We previously reported ultrafast near-field transient transmission (space/time resolution was *ca.* 50 nm/100 fs) of single gold nanorods to reveal dynamic behavior of the material.[2)] We used a near-infrared pulse to excite longitudinal plasmon resonance of the rod and detect transient transmission change after that. Figure 2A shows the transient image of a nanorod at *ca.* 600 fs. Although the rod consists of uniform crystalline gold, the signal is strongly dependent on the position: bleached absorption is observed in the central part, while induced absorption is found in both ends.

To understand the observed features, we simulated in the present study position-dependent transient transmission change based on electromagnetic LDOS calculation.[3)] Figure 2B shows a simulated image. The image reproduces well the observed features of the transient image in Figure 2A. From this analysis, it has been revealed that the LDOS change arises from variation in plasmon mode wavefunctions due to the photoinduced transient electronic temperature elevation in the nanorod. The present result suggests a potential for transient optical control of plasmon modes by photoexcitation of metal nanostructures.

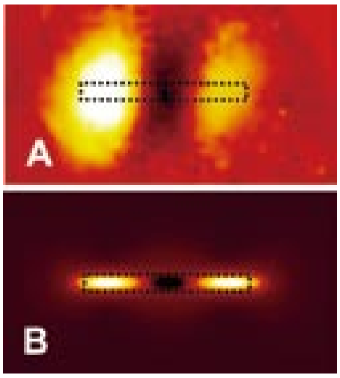

Figure 2. (A) Transient transmission image of a single gold nanorod (diameter 30 nm, length 300 nm) observed at a delay time of 600 fs. A dotted square indicates an approximate shape of the nanorod estimated from the topography measurement. Bright and dark parts indicate regions giving induced absorption and bleached absorption, respectively. (B) Simulated transient transmission (LDOS) change image for the nanorod. Bright and dark parts indicate regions giving enhanced and reduced LDOS, respectively.

3. Near-Field Imaging of Locally Enhanced Optical Fields in Metal Nanoparticle Assemblies

It is of fundamental importance to reveal spatial distribution of localized optical field in metal nanostructures. In aggregated noble metal nanoparticles, for example, strong electric field is expected in the interstitial gaps between the nanoparticles, according to the electromagnetic calculations. Such an enhanced optical field is considered as the major origin of the huge Raman enhancement in single-molecule level surface-enhanced Raman scattering (SERS). Recently, we visualized highly localized optical fields at interstitial sites in gold-nanoparticle dimers, by two-photon excitation imaging using SNOM.[4)] For larger nanostructures, however, the correlation between the geometrical structure and the optical field distribution has been less understood.

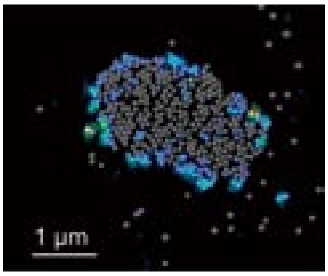

Figure 3. Two-photon excitation SNOM image of monolayer assembly of gold nanoparticles. The image is superimposed on the SEM image (displayed in black-white).

In this study, we analyzed the correlation between the near-field optical properties and the particle configuration in monolayer assemblies of gold nanoparticles by a combination of SNOM and SEM images (Figure 3).[5)] Two-photon excitation SNOM measurements show enhanced optical fields distributed over the whole area of assembly, and especially intensified at the rim of the assembly. The difference between the inner part and the rim may be related to delocalization of surface plasmon excitation in two-dimensional nanostructures. The non-uniform nature of the enhanced electric field in the assembly found here gives a new guideline for designing highly sensitive SERS substrate.

4. Near-Field Imaging of Organic Molecular Assemblies

We are studying mesoscopic structures and optical properties of organic molecular assemblies such as porphyrin wires, carbon nanotubes embedded in sugar molecule chains, Lagmuir-Blodgett films of functional conjugated molecules, mainly as collaborations with other research groups.

References

1) H. Okamoto and K. Imura, *Jpn. J. Appl. Phys.* **47**, 6055–6062 (2008).
2) K. Imura, T. Nagahara and H. Okamoto, *J. Phys. Chem. B* **108**, 16344–16347 (2004).
3) K. Imura and H. Okamoto, *Phys. Rev. B* **77**, 041401(R) (4 pages) (2008).
4) K. Imura, H. Okamoto, M. K. Hossain and M. Kitajima, *Nano Lett.* **6**, 2173–2176 (2006).
5) T. Shimada, K. Imura, M. K. Hossain, H. Okamoto and M. Kitajima, *J. Phys. Chem. C* **112**, 4033–4035 (2008).

---

* from KAIST, Korea

Quantum-State Manupulation of Molecular Motions

Department of Photo-Molecular Science
Division of Photo-Molecular Science I

OHSHIMA, Yasuhiro	Professor
HASEGAWA, Hirokazu	Assistant Professor
BAEK, Dae Yul	IMS Fellow
SUMA, Kosuke	JSPS Post-Doctoral Fellow*
PAVLOV, Lubomir	Visiting Scientist†
KITANO, Kenta	Graduate Student
MIYAKE, Shinichiro	Graduate Student
INAGAKI, Itsuko	Secretary

Molecules in gas phase undergo translational, rotational and vibrational motions in a random manner, and the total molecular system is a statistical ensemble that contains a number of molecules in many different states of motions. This research group aims to establish methods to manipulate the quantum-state distribution pertinent to molecular motions, by utilizing the coherent interaction with laser lights. Here lasers with ultimate resolution in time and energy domains are employed complementally and cooperatively for manipulation of molecular motions.

1. Nonadiabatic Rotational Excitation of Benzene by Nonresonant Intense Femtosecond Laser Fields1)

When a gaseous molecular sample is irradiated by an intense nonresonant ultrafast laser pulse, the laser field exerts a torque that aligns the molecular axis along the laser polarization vector, due to the interaction with the molecular anisotropic polarizability. The process has now been termed commonly as "nonadiabatic molecular alignment," and has been attracting much attention because of interesting physics involved and possible broader applications.2) Here the field–molecule interaction only remains in much shorter duration than the characteristic time for molecular rotation, and thus the nonadiabatic alignment is inherently accomplished by nonadiabatic rotational excitation (NAREX), where rotation of the molecules is coherently excited to create a rotational quantum wave packet (WP), a non-stationary superposition of rotational eigenstates.

We have recently developed a method for exploring the NAREX process in a quantum-state resolved manner by using resonance-enhanced multiphoton ionization (REMPI), and reported state distribution of NO molecules after the impulsive excitation with a fundamental output of a femtosecond titanium-sapphire laser.3) It has been shown that the state distribution is a useful experimental source for verifying the excitation process, since population for each rotational level is proportional to the square of the probability amplitude of the corresponding eigenstate in the rotational WP thus created.

The method has been further applied to the oblate symmetric-top molecule, benzene. Rotational excitation up to J = 10 was observed for the irradiation of a molecular ensemble, initially cooled to 0.5 K in an adiabatic expansion, by the femtosecond laser pulse with the intensity of 2.2 TW/cm^2 (Figure 1). The observed excitation was analyzed by the aid of quantum mechanical calculations. These calculations show the systematic change in the excitation pathways for different K, which is characteristic of NARAX in symmetric-top molecules.

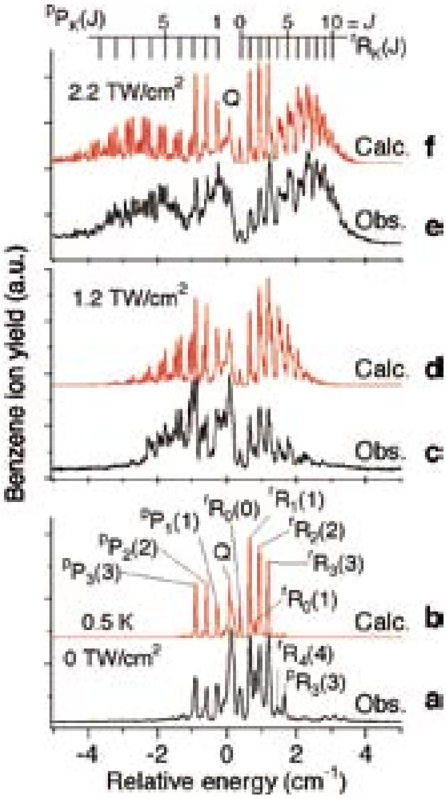

Figure 1. REMPI excitation spectra of the S_1–S_0 6_0^1 band of benzene. Observed (a) without pump pulses, (c) with the pump pulse of 1.25 mJ and (e) 2.40 mJ with 700 fs duration. Calculated with the laser intensities of (b) 0 TW/cm^2, (d) 1.2 TW/cm^2, and (f) 2.2 TW/cm^2.

2. Quantum State Reconstruction of a Rotational Wave Packet Created by a Nonresonant Intense Femtosecond Laser Field[4)]

We further succeeded in experimentally reconstructing a rotational WP created in the NAREX process by utilizing a nonresonant intense femtosecond laser field. Specifically, a rotational WP in an adiabatically cooled benzene molecule was determined. In this WP reconstruction, the initial WP was further interfered by a replica of the first laser pulse, and a REMPI probe was conducted to observe the resultant modulation in population. The time dependent population was fitted to determine the phases as well as the amplitudes of the WP, as shown in Figure 2. Though several states with different nuclear-spin modifications were populated in the initial condition, a single wave packet created from one of them (with $J = 0$) is specifically reconstructed owing to the state-selective probing. From the experimentally determined phases and amplitudes, the angular probability distribution can be evaluated, as shown in Figure 3.

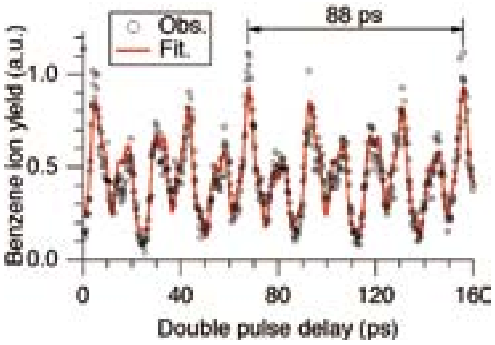

Figure 2. Population of the $J_{|K|} = 0_0$, state in benzene molecules after double-pulse excitation, plotted against the delay between the two pulses. Open circles represent the observed value, and the red line is the results from a least-squares fitting.

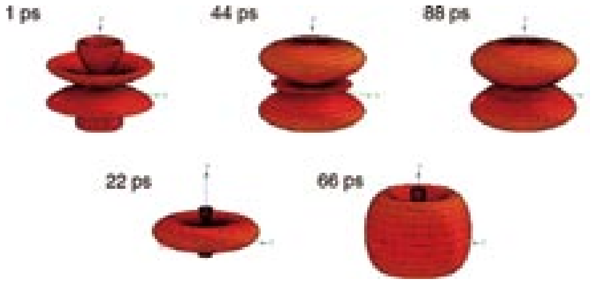

Figure 3. Angular probability distribution of the molecular symmetry axis of benzene at some delay times, evaluated from the experimentally determined amplitude and phase.

3. Realization of Nonadiabatic Vibrational Excitation by Nonresonant Intense Femtosecond Laser Fields

Nonadiabatic interaction with a nonresonant intense ultrafast laser field can also coherently excite the vibration of molecules. Realization of such a nonadiabatic vibrational excitation (NAVEX) and the resultant creation of a vibrational WP is definitely the next step to be proceeded. We have extended the research into this direction, and just recently succeeded in modifying the vibrational-state distribution by utilizing nonresonant intense femtosecond laser pulse(s).

4. Construction of Coherent ns Pulsed Light Sources for Adiabatic Population Transfer

Highly efficient population transfer between quantum states can be accomplished with adiabatic interactions with ns coherent laser pulses, such as stimulated Raman adiabatic passage.[5)] For realizing such an adiabatic quantum-state manipulation, we are constructing two independent laser systems, both of which will deliver pulsed outputs with almost Fourier-transform (FT) limited resolution. The first system, already in operation, is based on the pulsed amplification of the output from a cw ring titanium-sapphire laser.

The second laser system is based on the optical parametric oscillation (OPO) injection-seeded by an extra-cavity cw diode laser. We have succeeded in single-mode operation of the OPO system with the following characteristics: the laser bandwidth of 160 MHz (FWHM), the pulse duration of ~4 ns, and the output power of 7 mJ/pulse (at ~530 nm as the signal wave). Measurements of high-resolution excitation spectra of aromatic molecules are now underway by utilizing the single-mode OPO system.

References

1) H. Hasegawa and Y. Ohshima, *Chem. Phys. Lett.* **454**, 148–152 (2008).
2) H. Stapelfeldt and T. Seideman, *Rev. Mod. Phys.* **75**, 543–557 (2003).
3) H. Hasegawa and Y. Ohshima, *Phys. Rev. A* **74**, 061401 (4 pages) (2006).
4) H. Hasegawa and Y. Ohshima, *Phys. Rev. Lett.* **101**, 053002 (4 pages) (2008).
5) N. V. Vitanov, T. Halfmann, B. W. Shore and .K. Bergmann, *Annu. Rev. Phys. Chem.* **52**, 763–809 (2001).

* Present address: The University of Tokyo, Graduate School of Engineering, Department of Chemical System Engineering, Tokyo113-8656

† from Bulgarian Academy of Science

Development of High-Precision Coherent Control and Its Applications

Department of Photo-Molecular Science
Division of Photo-Molecular Science II

OHMORI, Kenji	Professor
KATSUKI, Hiroyuki	Assistant Professor
HOSAKA, Kouichi	IMS Fellow*
DELAGNES, Jean-Christophe	Post-Doctoral Fellow†
SHIMADA, Hiroyuki	Post-Doctoral Fellow
GOTO, Haruka	Graduate Student
INAGAKI, Itsuko	Secretary

Coherent control is based on manipulation of quantum phases of wave functions. It is a basic scheme of controlling a variety of quantum systems from simple atoms to nanostructures with possible applications to novel quantum technologies such as bond-selective chemistry and quantum computation. Coherent control is thus currently one of the principal subjects of various fields of science and technology such as atomic and molecular physics, solid-state physics, quantum electronics, and information science and technology. One promising strategy to carry out coherent control is to use coherent light to modulate a matter wave with its optical phase. We have so far developed a high-precision wave-packet interferometry by stabilizing the relative quantum phase of the two molecular wave packets generated by a pair of femtosecond laser pulses on the attosecond time scale. We will apply our high-precision quantum interferometry to gas, liquid, solid, and surface systems to explore and control various quantum phenomena.

1. Actively Tailored Spatiotemporal Images of Quantum Interference on the Picometer and Femtosecond Scales[1)]

Interference fringes of quantum waves weave highly regular space-time images, which could be seen in various wave systems such as wave packets in atoms and molecules, Bose Einstein condensates, and Fermions in a box potential. We have experimentally designed and visualized spatiotemporal images of dynamical quantum interferences of two counter-propagating nuclear wave packets in the iodine molecule; the wave packets are generated with a pair of femtosecond laser pulses whose relative phase is locked within the attosecond time scale. The design of the image has picometer and femtosecond resolutions, and changes drastically as we change the relative phase of the laser pulses, providing a direct spatiotemporal control of quantum interferences.

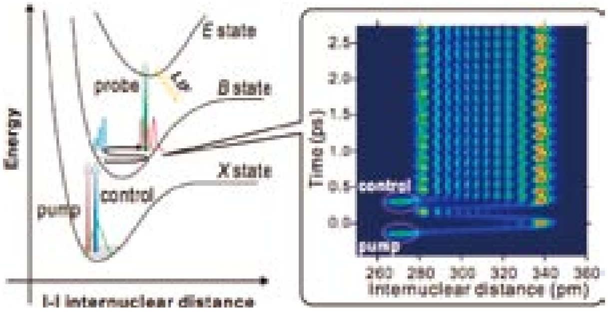

Figure 1. Pump-control-probe scheme for tailoring and visualizing the quantum carpet in the iodine molecule. (Left) Three femtosecond laser pulses are employed. Two of them are phase-locked and used as the pump and control pulses, and the other one is not phase-locked and is used as the probe pulse. The fluorescence signal induced by the probe pulse is measured with a photomultiplier tube attached to a monochromator. (Right) The model simulation of the quantum interference of two wave packets created on the *B*-state potential curve of the iodine molecule by the pump and control pulses. The interference shows a highly regular space-time image that looks like a carpet.

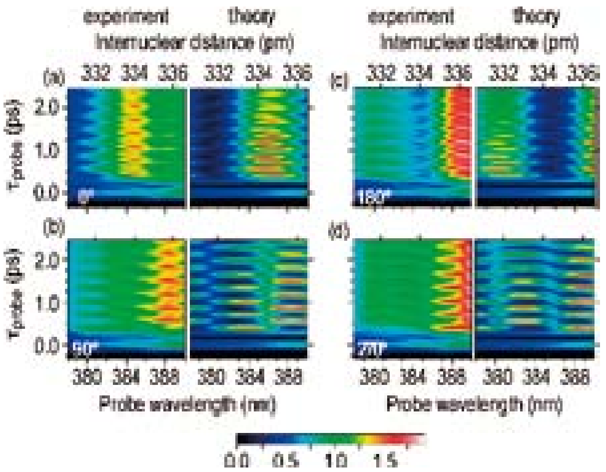

Figure 2. Comparisons of the quantum carpets measured (left) and simulated (right) at the pump-control relative phases θ_{pc} = (a) 0°, (b) 90°, (c) 180°, and (d) 270°. The color scaling is common within each set of measured or simulated carpets; the maxima of those two sets have the same color. The origin $\tau_{peobe} = 0$ of the simulated carpet denotes a position of the top of the first oscillation around the outer turning point. The simulations include the interactions with the pump, control, and probe pulses. The parameter $\tau_{control}$, used for the simulation of $\theta_{pc} = 0°$, was 468.920 fs.

Reference

1) H. Katsuki, H. Chiba, C. Meier, B. Girard and K. Ohmori, *Phys. Rev. Lett.* submitted.

* Present Affiliation; Postdoctral Fellow, Japan Atomic Energy Agency

† Present Affiliation; Senior Lecturer, The University of Bordeaux, France

Molecular Inner-Shell Spectroscopy: Electronic Structure and Intermolecular Interaction

Department of Photo-Molecular Science
Division of Photo-Molecular Science III

KOSUGI, Nobuhiro	Professor
YAMANE, Hiroyuki	Assistant Professor
NAGASAKA, Masanari	Assistant Professor
KIMBERG, Victor	Post-Doctoral Fellow
NAKANE, Junko	Secretary

In order to reveal electronic structure and intermolecular interaction of molecular solids, liquids, and clusters, we are developing and improving soft X-ray spectrometers for resonant Auger spectroscopy (RAS) and inelastic soft X-ray emission spectroscopy (XES). We are also developing and improving an original *ab initio* quantum chemical program package GSCF, which is optimized to calculation of molecular inner-shell processes.

1. Charge-Transfer- to-Solvent States of Aqueous Chloride Ions Revealed by Cl⁻ 2p Resonant Auger Spectroscopy[1)]

Charge transfer-to-solvent (CTTS) excited states of 2 mol/l NaCl and 3 mol/l LiCl aqueous solutions are revealed through soft X-ray electron spectroscopy. The excitation of the Cl 2p core electrons to the CTTS states is hardly visible in soft X-ray absorption spectroscopy. In this work it is clearly shown that the CTTS states can be detected by measuring RAS following the Cl 2p excitation to the CTTS state. During the resonance Auger decay emitting an Auger electron the CTTS electron behaves like a spectator; in the Auger final state with valence double holes, the CTTS electron gets strongly bound by a singly charged state and definitely observable.

The observed results are satisfactorily reproduced by *ab initio* calculations of four different cluster models to simulate about 2 mol/l NaCl and LiCl aqueous solutions, that is, 1 alkali halide and about 30 water molecules in a volume of (10 Å)^3. The initial guess of these geometries was chosen from a stable cluster of 30 H_2O molecules composed of five- and four-member water rings, where the center water molecule of this cluster was exchanged to either Cl or Na/Li. We chose two local minima for LiCl+29·H_2O and a local minimum for NaCl+29·H_2O and for NaCl+31·H_2O. In these clusters Cl^- is stabilized by five or six nearest-neighbor H_2O molecules. The theoretical method for the Cl 2p ionized states (to describe photoionization) and Cl 3p doubly ionized states (to describe Auger decay) is also an all-electron ab initio approach taking into account Cl 2p and Cl 3p holes explicitly, using the GSCF3 code. The energy levels corresponding to CTTS electrons bound by single and double hole states, which are optimized within the static exchange (STEX) method, simulate the experimental results quite well.

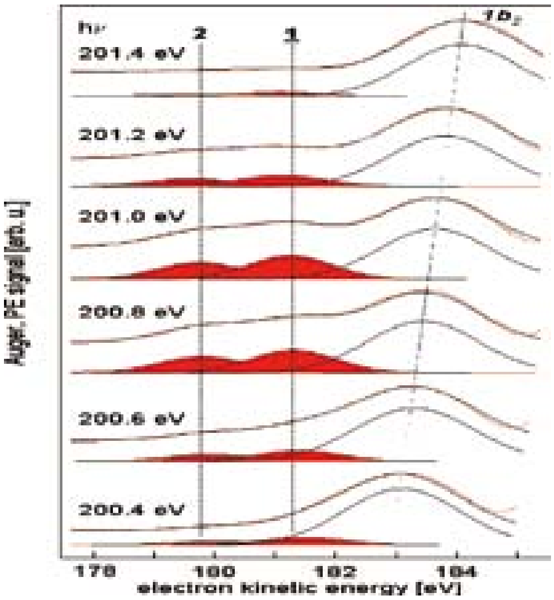

Figure 1. Photon energy dependence of electron kinetic energy spectra of resonant Auger electrons from the Cl 2p CTTS states in aqueous Cl^- ions and non-resonant photoelectrons from the liquid water $1b_2$ level.

As shown in Figure 1, we also have observed the small negative photon-energy dependence of the lowest spectator Auger electron, which indicates localized character of the lowest CTTS electron. Similar negative photon-energy dependence of the resonant Auger electron energy has been observed in molecular solid[2)] and DNA,[3)] and discussed in terms of localization and delocalization of the excitonic features.

The present liquid-jet experiments and *ab initio* calculations highlight the potential of combination of resonant inner-shell excitations with liquid photoelectron spectroscopy to explicitly characterize CTTS electron dynamics in aqueous solutions.

2. Exchange Interaction of Rydberg Electrons bound by Singly and Doubly Charged States in Small Kr Clusters[4)]

Similarly to the CTTS electron in aqueous solutions, the Rydberg electron in atomic van der Waals clusters is characterized by means of soft X-ray inner-shell spectroscopy. The Rydberg electron from neutral species is more strongly bound and more clearly observed than the CTTS electron from Cl^-.

Singly charged ion cores created by photoionization of atomic clusters are stabilized by the induced polarization (PL) interaction of the surrounding atoms, showing characteristic redshifts of the ionization energy. On the other hand, the photoexcitation creates Rydberg electrons bound by singly charged ion cores, as schematically shown in Figure 2(a). The photoexcitation energy sometimes shows blueshifts due to larger exchange (EX) interaction of a Rydberg electron with electrons of the surrounding atoms. Following the photoexcitation, the resonant Auger decay creates doubly charged ion cores with the Rydberg electron as a spectator. The doubly charged state can have four times larger PL interaction than the singly charged state. On the other hand, the EX interaction of Rydberg electrons is dependent on overlap of the wavefunctions, indicating that shrink of the Rydberg orbital in the doubly charged state increases more or less EX interaction.

Furthermore, small Kr clusters show surface site (‘corner,’ ‘edge,’ and ‘face’) dependent redshifts in ionization energy in X-ray photoelectron spectroscopy (XPS)[5)] and surface site dependent blueshifts and redshifts in excitation energy in x-ray absorption spectroscopy (XAS).[6)] In the present work, surface site dependent EX and PL interactions of small Kr clusters with an average size of Kr_{15} are investigated in doubly charged ion cores by resonant Auger spectroscopy (RAS), and compared by those in singly ionized core obtained by XAS.

Figure 2(b) shows XAS of Kr clusters at the Kr $3d_{5/2}$ edge. Several surface sites show different energy shifts at the 5p and 6p Rydberg states. The 5p electron has the largest EX interaction of the Rydberg states, because the radius of the 5p Rydberg orbital is close to the inter-atomic distance in Kr clusters and the higher Rydberg electron is more diluted in the cluster with decreasing overlap with the surroundings. It is also noted that the EX interaction is almost proportional to the nearest coordination number at the surface site.

Figure 2(c) shows RAS of Kr clusters in the $4s^{-1}4p^{-1}5p$ and $4p^{-2}6p$ regions after the ‘edge’ site excitation of the $3d_{5/2}{}^{-1}5p$ transition (91.37 eV). The EX interaction of the Rydberg electron in doubly charged ion core can be evaluated from the energy shift of RAS assuming the PL effect of the doubly charged ion is four times larger than that of the singly charged ion. Thus, we have found that the EX interaction of the Rydberg electron is greatly enhanced in the doubly charged ion core due to sudden shrink of the Rydberg orbital; the EX interaction of the 6p Rydberg electron with the doubly charged ion core is almost the same as EX of the 5p Rydberg with the singly charged ion core.

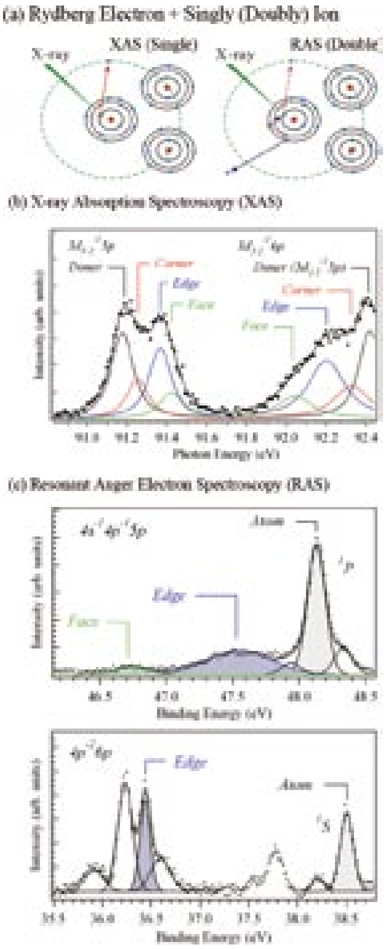

Figure 2. (a) Singly charged ion core and Rydberg electron as revealed by XAS. Doubly charged ion core and Rydberg electron as revealed by RAS. (b) Kr $3d_{5/2}$ XAS spectra of small Kr clusters in the $3d_{5/2}{}^{-1}5p$ and $3d_{5/2}{}^{-1}6p$ region. (c) RAS spectra of small Kr clusters in the $4s^{-1}4p^{-1}5p$ and $4p^{-2}6p$ region after the ‘edge’ site excitation of the $3d_{5/2}{}^{-1}5p$ transition (91.37 eV).

References

1) B. Winter, E. F. Aziz, N. Ottosson, M. Faubel, N. Kosugi and I. V. Hertel, *J. Am. Chem. Soc.* **130**, 7130 (2008).
2) Y. Takata, T. Hatsui and N. Kosugi, *J. Electron Spectrosc.* **88-91**, 235 (1998).
3) H. S. Kato, M. Furukawa, M. Kawai, M. Taniguchi, T. Kawai, T. Hatsui and N. Kosugi, *Phys. Rev. Lett.* **93**, 086403 (2004).
4) M. Nagasaka, T. Hatsui and N. Kosugi, *J. Electron Spectrosc.* **166-167**, 16 (2008).
5) T. Hatsui, H. Setoyama, N. Kosugi, B. Wassermann, I. L. Bradeanu and E. Rühl, *J. Chem. Phys.* **123**, 154304 (2005).
6) A. Knop, B. Wassermann and E. Rühl, *Phys. Rev. Lett.* **80**, 2302 (1998).

Extreme UV Photoionization Studies of Fullerenes by Using Synchrotron Radiation and High-Temperature Mass Spectrometer

Department of Photo-Molecular Science
Division of Photo-Molecular Science III

MITSUKE, Koichiro	Associate Professor
KATAYANAGI, Hideki	Assistant Professor
HUANG, Chaoqun	IMS Fellow
YAGI, Hajime	Post-Doctoral Fellow
KAFLE, Bhim Prasad	Graduate Student (–March ’08) Post-Doctoral Fellow (April ’08–)
NAKAJIMA, Koichi	Visiting Scientist*
PRODHAN, Md. Serajul Islam	Graduate Student

Interactions of C_{60}, C_{70}, C_{84} … with photons have attracted considerable attention, since fullerene family provide unique molecular systems characterized by exceptionally stable electronic structures associated with dense and highly degenerated molecular orbitals and by extremely large vibrational degrees of freedom. In UVSOR we succeeded in determining the total photoabsorption cross section curves of $C_{60(70)}$ at $h\nu$ = 1.3 to 42 eV by using photon attenuation method. Moreover, the yield curves of singly- and multiply-charged photoions from fullerenes were measured at $h\nu$ = 25 to 200 eV. We have studied the mechanisms and kinetics of sequential C_2-release reactions from the yield curves for $C_{60(70)-2n}{}^{z+}$ as a function of the internal energy of the parent $C_{60(70)}{}^{z+}$ ions. To gain more insight into the dissociation mechanisms we have constructed a velocity map imaging spectrometer for achieving the 3D velocity distributions of the fragments $C_{60(70)-2n}{}^{z+}$.

1. Photoabsorption Cross Section of C_{60} Thin Films from the Visible to Vacuum Ultraviolet[1)]

Absolute photoabsorption cross sections of C_{60} thin films are determined in the $h\nu$ range from 1.3 to 42 eV by using photon attenuation method. The spectrum shows a prominent peak of 1180 Mb at 22.1 eV with several fine structures due to single-electron excitation similarly to the case of C_{60} in the gas phase. The complex refractive index and complex dielectric function are calculated up to 42 eV through the Kramers-Kronig analyses. From the present data of C_{60} thin films the cross section curve of a molecular C_{60} is calculated with an assumption that the polarization effect of surrounding C_{60} molecules can be expressed by the standard Clausius-Mossotti relation. The spectrum thus obtained shows an excellent agreement with that of C_{60} in the gas phase measured independently.

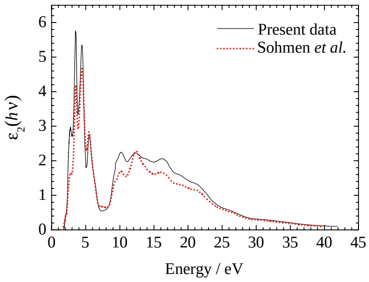

Figure 1. Dependences on $h\nu$ of $\varepsilon_2(\nu)$ of the complex dielectric function $\varepsilon(\nu) = \varepsilon_1(\nu) + i\varepsilon_2(\nu)$ of the C_{60} film.

2. Photoabsorption Cross Section of C_{70} Thin Films from the Visible to Vacuum Ultraviolet

Absolute photoabsorption cross sections of C_{70} thin films are determined in the $h\nu$ range from 1.3 to 42 eV by using photon attenuation method. The spectrum shows a prominent peak of 1320 Mb at 21.4 eV with several fine structures probably due to single-electron excitation. The complex refractive index and complex dielectric function are calculated up to 42 eV through the Kramers-Kronig analyses. From the present data of C_{70} thin films the cross section curve of a molecular C_{70} is calculated using the standard Clausius-Mossotti relation dealing with the correction of the local electromagnetic field, with a plausible assumption that the molecular rotation at room temperature could smear out the effect of the anisotropic molecular structure of C_{70}.

3. Performance Test of a New Velocity Map Imaging (VMI) Spectrometer[2)]

We have constructed a photoion imaging spectrometer to measure the velocity distributions of fragments produced by dissociative photoionization of fullerenes with synchrotron radiation. The performance of this spectrometer has been tested using rare gas samples at room temperature. We have compared the images experimentally obtained with those generated by a simulation program based on a field free expansion of photoions. The experimental and simulated images agree well with each other, if we assume the Maxwell-Boltzmann velocity distribution and the Gaussian distribution for the defocusing of the images with a standard deviation σ of 2 mm.

4. VMI of C_{60} Molecular Beams[3)]

The speed and angular distributions of C_{60} molecular beams have been determined by using a VMI technique for photoions produced by irradiation of synchrotron radiation. The C_{60} powder in the sample cell was heated and the beam was generated in an effusive condition. The two-dimensional projection of the velocity distribution was recorded (Figure 2) as an image on the position sensitive detector (PSD), and was converted to the speed and angular distributions. The speed distribution was expressed by the Maxwell-Boltzmann distribution at the temperature of the sample cell, while the angular distribution was determined by the geometry of the fullerene beam source. The speed distribution of helium in thermal motion was used to calibrate the velocity scale.

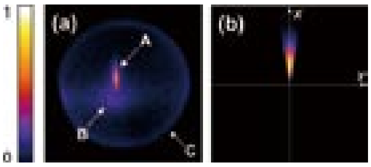

Figure 2. (a) Ion image of the fullerene beam at $h\nu$ = 70 eV. Pattern A is assigned to the signal of the C_{60} beam. (b) Ion image of the fullerene beam by computer simulation.

5. VMI Spectroscopy of Photofragments from C_{60} Beams

Simulations have been performed to calculate the scattering distributions of C_{56}^+ fragment ions produced by two different mechanisms of dissociative photoionization of C_{60}: (1) sequential ejection of C_2 units and (2) fission into C_{56}^+ + C_4. The simulated images for the two mechanisms can be distinguished clearly at T = 0 K, whereas their differences appear to be less obvious for bulk C_{60} at room temperature. Nevertheless, our VMI spectrometer is found to have an enough resolution under the beam condition to reveal such differences in the velocity distribution, because the transverse velocity of the beam is estimated to be less than 20 m s^{-1} even at T = 785 K.

6. Revision of our VMI Spectrometer[4)]

We have improved our earlier version of VMI spectrometer to be applied for measuring the momentum distributions of the fragments from fullerenes. The revised spectrometer is equipped with four electrostatic lens elements, a drift tube, a mass gate and a PSD. Application of an additional element to the conventional three-element lens system provides better focusing of an extended interaction region. Moreover, the electric field in the ionization region is kept cylindrically symmetric in spite of the field penetration from the oven and surface thickness monitor. The optimum arrangement and dimensions of the elements are determined from the calculations of ion trajectories of C_{56}^+, C_{58}^+ and C_{60}^+.

7. Measurements of Incident Photon-to-Current Efficiency (IPCE) and Photoabsorbance of Dye-Sensitized Solar Cells

We have fabricated dye-sensitized solar cells (DSC) comprised of Ru535 dye and PN50 electrolyte and measured their short current and the intensity of the transmitted light to estimate the wavelength dependence of the incidence photon-to-current efficiency (IPCE) and photoabsorbance (ABS) in the range of 300 to 1000 nm. In addition, we evaluated the quantum yield (EIQY) of DSCs for the electron injection from the excited orbital of Ru535 dye to the conduction band of TiO_2 nano particles. Our final goal is to develop DSCs with high performance and long lifetime by improving mainly ABS and EIQY in the near infrared region.

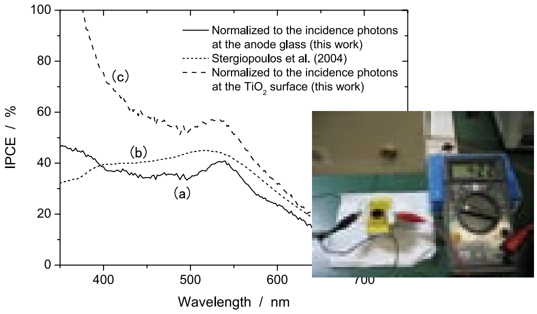

Figure 3. IPCE curves of dye-sensitized solar cells comprised of Ru535 dye and PN50 electrolyte. Normalization is made to the incidence light either (a) at the anode FTO glass or (c) at the TiO_2 surface. (b) Reported by Stergiopoulos *et al.* in 2004.

References

1) H. Yagi, K. Nakajima, K. R. Koswattage, K. Nakagawa, C. Huang, Md. S. I. Prodhan, B. P. Kafle, H. Katayanagi and K. Mitsuke, *Carbon* in press.

2) Md. S. I. Prodhan, H. Katayanagi, C. Huang, H. Yagi, B. P. Kafle and K. Mitsuke, *Chem. Phys. Lett.* in press.

3) H. Katayanagi, C. Huang, H. Yagi, B. P. Kafle, Md. S. I. Prodhan, K. Nakajima and K. Mitsuke, *Rev. Sci. Instrum.* submitted.

4) B. P. Kafle, H. Katayanagi, C. Huang, Md. S. I. Prodhan, H. Yagi and K. Mitsuke, *Nucl. Instrum. Methods Phys. Res., Sect. A* to be submitted.

---

* from Hosei University

Atoms & Molecules in Few-Cycle Intense Laser Fields

Department of Photo-Molecular Science
Division of Photo-Molecular Science III

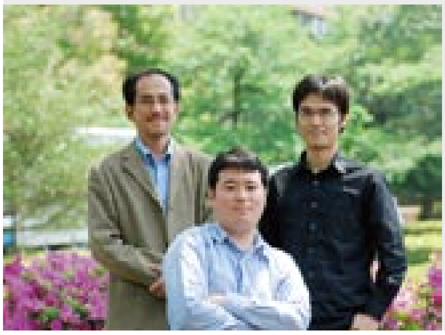

HISHIKAWA, Akiyoshi	Associate Professor
FUSHITANI, Mizuho	Assistant Professor
MATSUDA, Akitaka	IMS Fellow*
NAKANE, Junko	Secretary

Intense laser fields, comparable in magnitude with the Coulomb field within atoms and molecules, can be generated by focussing high-energy and ultrashort laser pulses. When exposed to such an intense laser field, molecules exhibit various exotic features that cannot be observed in weak laser fields. We are seeking a deeper understanding of the behavior of molecules in intense laser fields, to elucidate how molecules interact with light, as well as to apply the new features they exhibit to the real-time visualization of ultrafast chemical reactions and their control. In particular, we focus on the following research themes:

(1) Understanding of atomic and molecular dynamics in intense laser fields
(2) Ultrafast reaction imaging by laser Coulomb explosion imaging
(3) Generation and application of ultrashort soft-X-ray pulses by laser high-order harmonics.

1. Visualizing Recurrently Migrating Hydrogen in Acetylene Dication by Ultrashort Intense Laser Pulses[1,2)]

Highly charged molecular ions formed in ultrashort intense laser fields subsequently explode into fragments due to the strong electrostatic repulsion among the positive charges. The structure of the molecules at the instance of the laser irradiation can be studied by measuring precisely the momenta of the fragments. This can be compared to fireworks exploded in the night sky, which reflect how the “stars” containing sparklers are embedded in the shells. We studied the location of hydrogen atoms in deuterated acetylene dication, by igniting the “molecular fireworks” at different times after the creation of dication. We demonstrate the visualization of ultrafast hydrogen migration in deuterated acetylene dication ($C_2D_2^{2+}$) by employing the pump-probe Coulomb explosion imaging with sub-10-fs intense laser pulses (9 fs, 0.13 PW/cm^2, 800 nm). It is shown, from the temporal evolution of the momenta of the fragment ions produced by the three-body explosion, $C_2D_2^{3+} \rightarrow D^+ + C^+ + CD^+$, that the migration proceeds in a recurrent manner: The deuterium atom first shifts from one carbon site to the other in a short time scale (~90 fs) and then migrates back to the original carbon site by 280 fs, in competition with the molecular dissociation. Hydrogen migration plays important roles in various chemical reactions such as the synthesis of vitamin D in skin. The direct visualization demonstrated here will provide a deeper understanding of such chemical reactions as well as new prospects for their control.

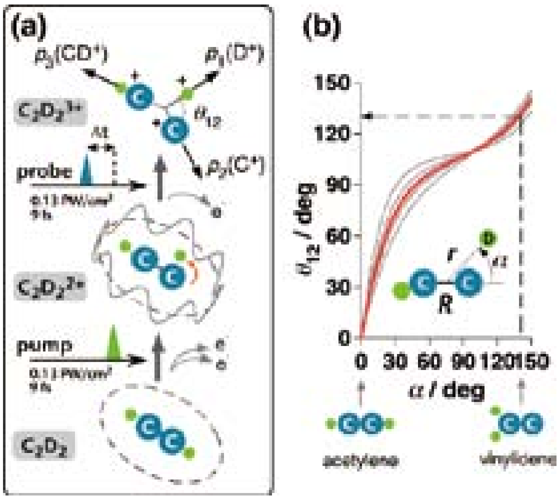

Figure 1. (a) Pump-probe Coulomb explosion imaging employed in the present study. The pump pulse creates $C_2D_2^{2+}$ and triggers the hydrogen migration. The instantaneous location of migrating deuterium atoms is determined from the momenta of fragment ions, D^+, C^+, CD^+, ejected in the Coulomb explosion of $C_2D_2^{3+}$ induced by the probe pulse. (b) Momentum angle θ_{12} as a function of the polar angle α obtained by classical simulation of the three-body Coulomb explosion.

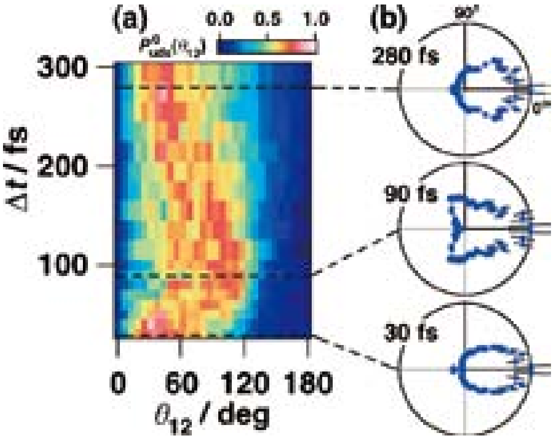

Figure 2. (a) Evolution of the momentum angle (θ_{12}) distribution and (b) the polar plot, showing the recurrent hydrogen migration in $C_2D_2^{2+}$.

2. Acetylene-Vinylidene Isomerization in Ultrashort Intense Laser Fields Studied by Triple-Ion Coincidence Momentum Imaging[3)]

Polyatomic molecules exposed to intense laser fields exhibit a variety of characteristic features associated with their many degrees of vibrational freedom. Due to the strong interaction with the laser fields, the geometrical structure can be strongly deformed by bond stretching or bending, and by isomerization through the rearrangement of chemical bonds. Hydrogen migration is one such processes, in which hydrogen atoms shift from one site to another within a molecule. Because of their large mobility, hydrogen atoms can explore the potential energy surfaces over long distances within the ultrashort laser pulse, leading to the formation of molecular hydrogen ion and the emission of energetic protons. In the present study, the isomerization of acetylene via hydrogen migration in intense laser fields (8×10^{14} W/cm^2) has been investigated by coincidence momentum imaging of the three-body Coulomb explosion process, $C_2H_2^{3+} \rightarrow H^+ + C^+ + CH^+$.

When ultrashort (9 fs) laser pulse are used, the angle between the momenta of C^+ and H^+ fragments exhibits a sharp distribution peaked at a small angle (~20°), showing that the hydrogen atom remains near the original carbon site in the acetylene configuration. On the other hand, a significantly broad distribution extending to larger momentum angles (~120°) is observed when the pulse duration is increased to 35 fs, showing that the ultrafast isomerization to vinylidene is induced in the longer laser pulse.

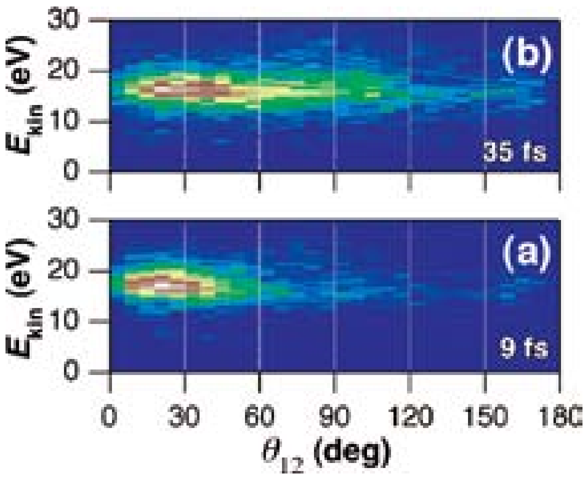

Figure 3. Two-dimensional maps of the momentum angle 12 between $\boldsymbol{p}_1(H^+)$ and $\boldsymbol{p}_2(C^+)$ and the total kinetic energy release for the asymmetric three-body Coulomb explosion process, $C_2H_2^{3+} \rightarrow H^+ + C^+ + CH^+$, observed for the (a) 9 fs and (b) 35 fs intense laser fields 8×10^{14} W/cm^2.

References

1) A. Hishikawa. A. Matsuda, M. Fushitani and E. J. Takahashi, *Phys. Rev. Lett.* **97**, 258302 (2007).
2) A. Hishikawa. A. Matsuda, M. Fushitani and E. J. Takahashi, *J. Phys.: Conf. Series* **88**, 012056 (2007).
3) A. Hishikawa, A. Matsuda, E. J. Takahashi and M. Fushitani, *J. Chem. Phys.* **128**, 084302 (2008).

---

* Present Address; Department of Physics, Stockholm University, Stockholm, Sweden

Light Source Developments by Using Relativistic Electron Beams

UVSOR Facility
Division of Advanced Accelerator Research

KATOH, Masahiro	Professor
ADACHI, Masahiro	Assistant Professor
SHIMADA, Miho	IMS Fellow*
TANIKAWA, Takanori	Graduate Student
KOIKE, Masashi	Graduate Student†
SUZUKI, Yasuhiro	Graduate Student†
YOSHIDA, Mitsuhiro	Graduate Student†
NAGATANI, Atsumune	Graduate Student†
FURUI, Yuta	Graduate Student†

This project involves researches and developments on synchrotron light source, free electron laser, beam physics and related technologies. Most of these works are performed at the UVSOR-II electron storage ring and its injector.

1. Developments on UVSOR-II Accelerators

Even after the major upgrade in 2003,1) the UVSOR-II electron storage ring and its injector have been continuously improved. In these years, the ring has been operated with a small emittance of 27 nm-rad, that enables four undulators to produce highly brilliant synchrotron radiation in the VUV region. This small emittance, on the other hand, makes the beam lifetime short through the intrabeam scattering, so called Touschek effect. To solve this lifetime problem eternally, we are preparing for top-up injection scheme. In this scheme, the electron beam is re-filled with a short interval, typically one minute, to keep the beam current almost constant.

To realize the top up injection, the maximum operating energy of the injector and the beam transport line was increased from 600 MeV to 750 MeV, by reinforcing the magnet power supplies. Since July, 2007, we have been operating the ring with full energy injection in the user runs. Generally, during injections, the beam loss rate becomes higher. An interlock system for the radiation safety is being developed, which limits the number of injected electrons. Test operation of the top-up scheme will be started in September, 2008.

2. Storage Ring Free Electron Laser

The low emittance and the high peak current of UVSOR-II enable the free electron laser to oscillate in the deep UV region with high output power exceeding 1W.2) In 2007, the shortest wavelength has reached 199 nm. Lasing around 190 nm will be tried soon.

Several users' experiments using this high power and tunable laser beam in the deep UV are in progress. However, during the high power operation of the free electron laser, a rapid change of the output power was observed, which was presumably due to the thermal deformation of the mirrors of the optical cavity. A feedback system is being developed to stabilize the output power.

Table 1. Parameters of UVSOR-II Free Electron Laser.

Electron Energy	600–750 MeV
Wave Length	800–199 nm
Spectral Band Width	$\sim 10^{-4}$
Polarization	Linear/Circular
Repetition Rate	11.26 MHz
Average Output Power	~1 W

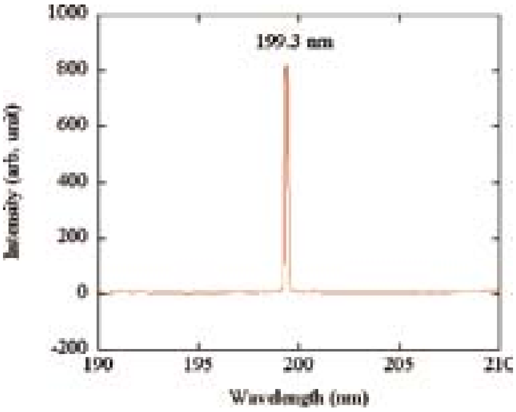

Figure 1. Successful lasing at 199.3 nm of UVSOR-II Free Electron Laser.

3. Terahertz Coherent Synchrotron Radiation by Laser-Electron Interaction

When an electron bunch has a micro-structure on its longitudinal density distribution whose typical scale is close to the radiation wavelength, the synchrotron radiation fields

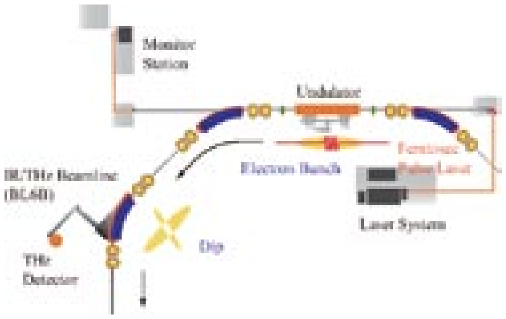

Figure 2. Laser Modulation System at UVSOR-II.

emitted by each electron are linearly accumulated and the total radiation power is proportional to the square of the number of the electrons. This is called coherent synchrotron radiation (CSR).

We have developed a system to create micro-density structure on electron bunches circulating in the storage ring, as shown in Figure 2.[3] Laser pulses are injected to the ring and interact with the electron beam in an undulator. The electrons lose or gain its energy depending on the phase to the laser field. As the result, energy modulation is created on the electron bunch. As the bunch is proceeding in the ring, the energy modulation is converted to a density modulation. By controlling the laser pulse shape, we can create various density structures. When we use a sub-picosecond laser pulse, we can produce a short dip structure. When we use a amplitude modulated laser pulse, we can produce periodic density structure. In the former case, broadband coherent terahertz radiation was produced.[3] In the latter case, quasi-monochromatic coherent terahertz radiation was produced, as shown Figure 3.[4] This was the first experiment in which monochromatic synchrotron radiation was produced in a uniform magnetic field.

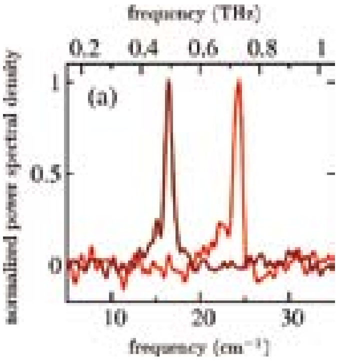

Figure 3. Quasi-monochromatic synchrotron radiation emitted in a uniform magnetic field.

4. Coherent Harmonic Generation

Coherent harmonic generation is a method to produce coherent harmonics of laser light by using relativistic electron beam. The laser-electron interaction in an undulator produces density modulation of a period of laser wavelength. When the energy modulation is sufficiently larger than the natural energy spread, the density modulation contains higher harmonic component of the laser wavelength. Such an electron bunch emits coherent harmonics of the injected laser. We have successfully observed the coherent third harmonics of Ti:Sa laser.[5] Optical properties of the coherent harmonic radiation were experimentally investigated.

References

1) M. Katoh, M. Hosaka, A. Mochihashi, J. Yamazaki, K. Hayashi, Y. Hori, T. Honda, K. Haga, Y. Takashima, T. Koseki, S. Koda, H. Kitamura, T. Hara and T. Tanaka, *AIP Conf. Proc.* **705**, 49–52 (2004).
2) M. Hosaka, M. Katoh, A. Mochihashi, M. Shimada, T. Hara and Y. Takashima, *Proc. 28th Internat. Free Electron Laser Conf. (Berlin)* 368–370 (2006).
3) M. Shimada, M. Katoh, S. Kimura, A. Mochihashi, M. Hosaka, Y. Takashima, T. Hara and T. Takahashi, *Jpn. J. Appl. Phys.* **46**, 7939–7944 (2007).
4) S. Bielawski, C. Evain, T. Hara, M. Hosaka, M. Katoh, S. Kimura, A. Mochihashi, M. Shimada, C. Szwaj, T. Takahashi and Y. Takashima (in alphabetic order), *Nat. Phys.* **4**, 390–393 (2008).
5) M. Labat, M. Hosaka, A. Mochihashi, M. Shimada, M. Katoh, G. Lambert, T. Hara, Y. Takashima and M. E. Couprie, *Eur. Phys. J. D* **44**, 187–200 (2007) (Highlighted Paper).

---

* Present Address; High Energy Accelerator Research Organization (KEK), Tsukuba, 305-0801

† carrying out graduate research on Cooperative Education Program of IMS with Nagoya University

Synchrotron Radiation Spectroscopy on Strongly Correlated Electron Systems

UVSOR Facility
Division of Advanced Solid State Physics

KIMURA, Shin-ichi	Associate Professor
ITO, Takahiro	Assistant Professor
TERASHIMA, Kensei	JSPS Post-Doctoral Fellow
IM, Hojun	Post-Doctoral Fellow[*]
TSUNEKAWA, Masanori	Post-Doctoral Fellow[†]
MIZUNO, Takafumi	Graduate Student
IIZUKA, Takuya	Graduate Student
MIYAZAKI, Hidetoshi	Graduate Student[‡]
MATSUI, Takafumi	Graduate Student[‡]

Solids with strong electron–electron interaction, so-called strongly correlated electron systems (SCES), have a various physical properties, such as non-BCS superconducting, colossal magneto-resistance, heavy fermion and so on, which cannot be predicted by a first-principle band structure calculation. Thanks to the physical properties, the materials are the candidates of the next generation functional materials. We are investigating the mechanism of the physical properties of SCES, especially rare-earth compounds, organic superconductors and transition-metal compounds, by infrared/THz spectroscopy and angle-resolved photoemission spectroscopy using synchrotron radiation. Since experimental techniques using synchrotron radiation are evolved rapidly, the development of the synchrotron radiation instruments is also one of our research subjects.

1. Direct Observation of Dispersive Kondo Resonance Peaks in a Heavy-Fermion System1)

In heavy-fermion Ce compounds, it is widely accepted that a localized Ce 4f electron due to the strong correlation forms a sharp Kondo resonance (KR) peak just above the Fermi level through the hybridization with an itinerant conduction electron. As a function of this hybridization, the ground state varies from a magnetic to nonmagnetic heavy-fermion separated by a quantum critical point, revealing two characteristic energy scales: the Kondo temperature (T_K) and coherent temperature (T^*). However, an accurate electronic structure for the Ce 4f state has remained a long debated issue since the discovery of the heavy-fermion system in 1970's. Then we carried out the Ce 4d-4f resonant angle-resolved photoemission spectroscopy to study the electronic structure of strongly correlated Ce 4f electrons in a quasi-two-dimensional nonmagnetic heavy-fermion system $CeCoGe_{1.2}Si_{0.8}$. For the first time, dispersive coherent KR peaks of an f state crossing the Fermi level are directly observed together with the hybridized conduction band. Moreover, the experimental band dispersion is quantitatively in good agreement with a simple hybridization-band picture based on the periodic Anderson model. The obtained physical quantities, *i.e.*, T^*, T_K, and mass enhancement, are comparable to the results of thermodynamic measurements. These results manifest an itinerant nature of Ce 4f electrons in heavy-fermion systems and clarify their microscopic hybridization mechanism.

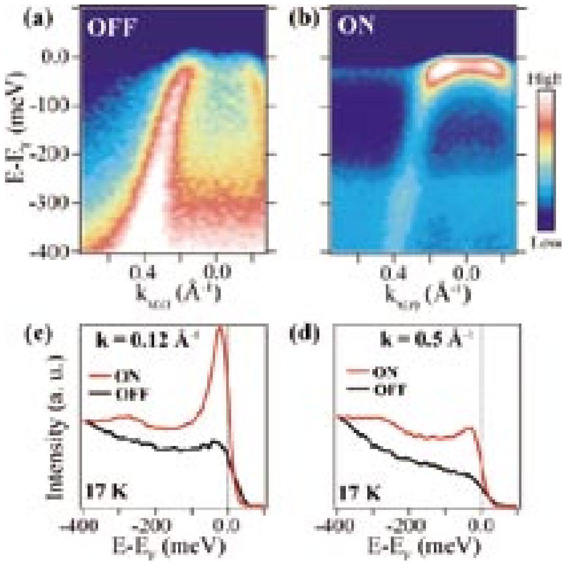

Figure 1. (a), (b) Intensity plots of off- and on-resonant ARPES spectra of $CeCoGe_{1.2}Si_{0.8}$ represent the band dispersion of conduction and f electrons, respectively, along the RT line. (c), (d) EDCs of on- and off-resonant ARPES spectra at the momentum k = 0.12 and 0.5 $Å^{-1}$, respectively.

2. Excitonic Instability in the Transition from the Black Phase to the Golden Phase of SmS under Pressure Investigated by Infrared Spectroscopy2,3)

In the translocation process from the local to itinerant character of carriers in strongly correlated electron systems, the physical properties drastically change due to the complex relation of the transport to magnetic properties. A strongly correlated insulator, samarium monosulfide (SmS), is a semiconductor with an energy gap size of ~1000 K (~90 meV) and its color is black (namely, the "black phase") at ambient pressure.[2] Above the critical pressure (P_c) of 0.65 GPa, the sample color changes to golden-yellow (the "golden phase") and the electrical resistivity then suddenly drops to one-tenth that in the black phase. To investigate the origin of the pressure-induced phase transition from the black phase to the golden phase, we measured the pressure-dependent optical reflectivity spectra of SmS in the far- and middle-infrared regions. The energy gap becomes narrow with increasing pressure in the black phase. A valence transition from Sm^{2+} in the black phase to mainly Sm^{3+} in the golden phase accompanied by spectral change from insulator to metal were observed at the transition pressure of 0.65 GPa. The black-to-golden phase transition occurs when the energy gap size of black SmS becomes the same as the binding energy of the exciton at the indirect energy gap before the gap closes. This result indicates that the valence transition originates from an excitonic instability.

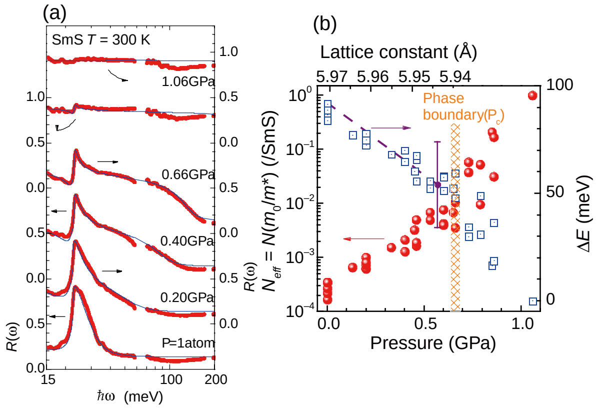

Figure 2. (a) Pressure dependence of the reflectivity spectrum [$R(\omega)$] of black SmS (thick lines) in the energy region of $\hbar\omega$ = 15–200 meV at 300 K. The fitting curve of the combination of Drude and Lorentz functions (thin lines) are also plotted. Successive curves are offset by 0.5 for clarity. (b) Pressure dependences of the effective carrier density (N_{eff}, solid circles) evaluated from the Drude and Lorentz fitting in the left figure and energy gap size (ΔE, open squares) evaluated from N_{eff} and ΔE at 1 atm. The lattice constant that is proportional to the pressure is also denoted in the figure for reference. The energy shift of the exciton peak of the direct transition at the X point at around 0.5 eV (dashed line) normalized at the energy gap size at ambient pressure are plotted as well.

3. Valence Electronic Structure of Cross-Linked C_{60} Polymer: In situ High-Resolution Photoelectron Spectroscopic and Density-Functional Studies[4]

When a C_{60} film is irradiated with a 3 keV electron beam, a cross-linked C_{60} polymer is formed and exhibits metallic electron-transport (I-V) properties in air at room temperature. To elucidate the origin of the metallic I-V characteristics of the cross-linked polymer, we examined the valence photoelectron spectra of the polymer using in situ high-resolution ultraviolet photoelectron spectroscopy (UPS) and found that the spectrum for the cross-linked C_{60} polymer came across the Fermi level (E_F). To understand the UPS results for the C_{60} polymer, we performed first-principles calculations of the band structure for three kinds of optimized three-dimensional unit cells of one-dimensional (1D) cross-linked C_{60} polymers with a cross-linkage consisting of both six- and seven-membered rings and of five- and eight-membered rings (P58). It was found that one quasi-1D P58 cross-linked C_{60} polymer shows semimetallic properties, which provides one possible explanation of both previous (metallic I-V characteristics) and present (valence photoelectron spectra) experimental results.

References

1) H. J. Im, T. Ito, H. -D. Kim, S. Kimura, K. E. Lee, J. B. Hong, Y. S. Kwon, A. Yasui and H. Yamagami, *Phys. Rev. Lett.* **100**, 176402 (2008).
2) S. Kimura, T. Mizuno, K. Matsubayashi, K. Imura, H. S. Suzuki and N. K. Sato, *Physica B* **403**, 805–807 (2008).
3) T. Mizuno, T. Iizuka, S. Kimura, K. Matsubayashi, K. Imura, H. S. Suzuki and N. K. Sato, *J. Phys. Soc. Jpn.* **77**, 113704 (2008).
4) J. Onoe, T. Ito, S. Kimura, K. Ohno, Y. Noguchi and S. Ueda, *Phys. Rev. B* **75**, 233410 (2007).

Awards

KIMURA, Shin-ichi; The Prize for Science and Technology in Research Category, the Commendation for Science and Technology by the Minister of Education, Culture, Sports, Science and Technology.
MIYAZAKI, Hidetoshi; Best Presentation Award, JSR 08.
MIYAZAKI, Hidetoshi; Best Presentation Award, Annual meeting of Tokai Branch of Japan Institute of Metals.

---

* from Sungkyunkwan University, Korea

† from Nagoya University

‡ carrying out graduate research on Cooperative Education Program of IMS with Nagoya University

Electronic Structure and Decay Dynamics in Atoms and Molecules Following Core Hole Creation

UVSOR Facility
Division of Advanced Photochemistry

SHIGEMASA, Eiji Associate Professor
HIKOSAKA, Yasumasa Assistant Professor

The dynamics of the inner-shell photoexcitation, photoionization, and subsequent decay processes is much more complex, in comparison to outer-shell photo-processes. For instance, the inner-shell photoionization is concomitant with the excitation and ionization of valence electrons, which reveal themselves as shake-up and shake-off satellite structures in the corresponding photoelectron spectrum. The one-photon multi-electron processes, which are entirely due to the electron correlation in the system, are known to happen not only in the primary inner-shell hole creation processes, but also in their relaxation processes. Our research project is focused on elucidating the electronic structures and decay dynamics in core-excited atoms and molecules, by utilizing various spectroscopic techniques together with monochromatized synchrotron radiation in the soft x-ray region.

1. Dissociation Dynamics in Polyatomic Molecules Following Core Hole Creation

Auger decay is the main relaxation process following core ionization in molecules composed of light atoms. In the decay process, a valence electron fills the core-hole while another valence electron is ejected. Doubly charged molecular ions with two holes in the valence shell, thus formed, often break up into ion fragments, due to the Coulomb repulsion between the nuclear charges. The coincidence detection between the energy-selected Auger electrons and fragment ions is one of the most powerful methods to gain a close insight into the dissociation mechanism of the Auger final states. To realize efficient coincidences among these charged particles, we have developed an Auger electron-ion coincidence spectrometer which consists of a double toroidal electron analyzer and a three-dimensional ion momentum spectrometer.

The Auger electron emission from the S $2p^{-1}$ core-hole states of OCS and subsequent dissociation processes of the doubly charged states have been investigated. The measurement has provided direct correlation between the doubly charged ion states and the dissociation pathways. The lowest-lying $(3\pi)^{-2}$ states located at about 32 eV binding energy produce the metastable OCS^{2+} and their lifetimes are expected to be much longer than 3.5 μs. The $(9\sigma)^{-1}(3\pi)^{-1}$, $(8\sigma)^{-1}(3\pi)^{-1}$ and $(2\pi)^{-1}(3\pi)^{-1}$ states around 36 eV are associated with both the formation of metastable OCS^{2+} and the dissociation into CO^+ + S^+. The three-body dissociation into O + C^+ + S^+ originates only from the high-lying states above 42 eV, whose main configurations are $(9\sigma)^{-2}$ and $(8\sigma)^{-1}(9\sigma)^{-1}$.

In order to investigate the influence of the localized core-hole creation to the formation of the valence two-hole states, and to elucidate their characters, the Auger decays following the C 1s and O 1s ionization in OCS have also been studied by using the same experimental setup. It was found that the lowest-lying $(3\pi)^{-2}$ states related to the production of the metastable OCS^{2+} are formed mainly via the Auger decay from the S $2p^{-1}$ core-hole states, which is explained by the localized nature of the 3π molecular orbital at the S atom.

2. One-Photon Multi-Electron Emission Processes Studied by Multi-Eelectron Coincidence Spectroscopy

When an inner-shell electron in atoms and molecules is removed, the core-hole state decays via the Auger electron transition. The kinetic energy of the Auger electron is element specific and therefore Auger electron spectroscopy is widely used as a powerful analytical tool in many different fields of research or even application. However, the detailed interpretation of the measured Auger spectra is difficult, even for atoms and small molecules. This is because inner-shell ionization of atoms and molecules is concomitant with the excitation and ionization of valence electrons, and all these core-hole states contribute to the conventional Auger electron spectra. Recently, we have successfully applied a magnetic bottle electron spectrometer to multi-electron coincidence spectroscopy for different systems.$^{1–4)}$ We describe here the results for the photoelectron-Auger-electron coincidence study in N_2 molecules, where the Auger decays from the individual inner-shell satellite states have been revealed.$^{1)}$

Figure 1(a) displays a two-dimensional (2D) map showing coincidences between 1s photoelectrons and Auger electrons. The conventional photoelectron and Auger electron spectra are plotted in Figures 1(b) and 1(c), respectively. Here the photoelectron spectrum is plotted in a binding energy scale relative to the $1s^{-1}$ state (409.94 eV). Inner-shell satellite structures (S_1–S_4) as well as the 1s mainline are clearly observed in the photoelectron spectrum. The 2D map shows horizontal structures at the 1s main line and the satellite states, which correspond to the Auger decays of these states. The decay mechanisms of the individual satellite states have been examined by extracting the coincidence Auger spectra from the 2D map. The decay features of the satellite states can be interpreted as spectator and participator behavior of the excited electrons.

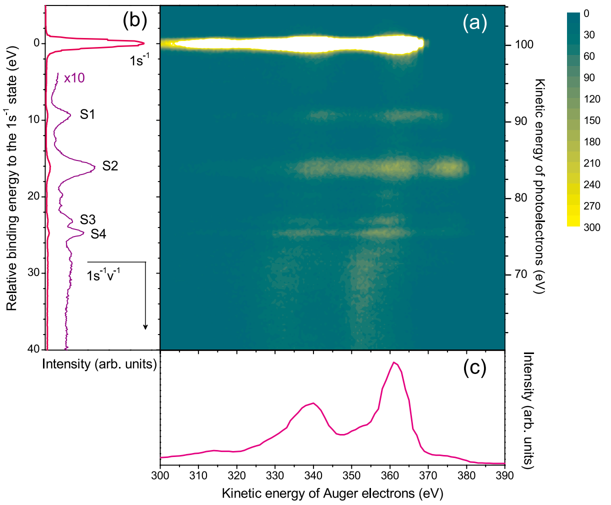

Figure 1. (a) Two-dimensional map of electron-electron coincidences, represented as a function of kinetic energies of photoelectrons and Auger electrons. (b) Conventional N 1s photoelectron spectrum. (c) Conventional Auger electron spectrum.

3. X-Ray Absorption Spectroscopy Measured in Resonant Auger Scattering Mode

The element specific information obtained by x-ray absorption spectroscopy (XAS) has a long history of application in various fields of research. A well-known bottleneck for XAS is the rather poor spectral resolution caused by the lifetime broadening of the core-excited states. Thanks to the rapid technological development related to synchrotron radiation, the possibilities of super-high resolution beyond the inherent lifetime widths have attracted considerable interest. The simple idea behind XAS with super-high resolution is to measure x-ray absorption in resonant x-ray Raman scattering (RXRS) or resonant Auger scattering (RAS) modes. Thus, an immediate advantage can be taken from the fact that the spectral resolution of RXRS and RAS is independent of the lifetime broadening of the core-excited states. The width of the XAS resonance in resonant scattering mode is then determined by the spectral function width of the incident x-ray radiation. Sharpening of the x-ray absorption resonances was indeed experimentally evidenced by scanning over the incident photon energy of these scattering processes within fixed narrow scattered-energy windows.

Recently it has been demonstrated that the super-narrow x-ray absorption profiles obtained in the RAS mode for the CO molecules give wrong resonance positions, owing to the lifetime vibrational interference between coherently populated core-excited levels.$^{5)}$ Figure 2 denotes the 2D map of the resonant Auger scattering yields, as a function of photon energy and electron kinetic energy, measured around the O1s → 2π resonance. The slight deviations of the positions of the hilltops from the vibrational progression of the core excited state can be seen in Figure 2.

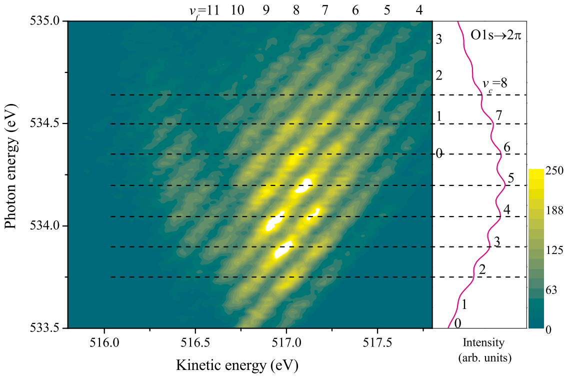

Figure 2. Two-dimensional map of the resonant Auger scattering yields from CO as a function of photon energy and electron kinetic energy, measured around the O1s → 2π resonance.

References

1) T. Kaneyasu, Y. Hikosaka, E. Shigemasa, F. Penent, P. Lablanquie, T. Aoto and K. Ito, *J. Phys. B* **40**, 4047–4060 (2007).

2) Y. Hikosaka, P. Lablanquie, F. Penent, T. Kaneyasu, E. Shigemasa, J. H. D. Eland, T. Aoto and K. Ito, *Phys. Rev. A* **76**, 032708 (6 pages) (2007).

3) T. Kaneyasu, Y. Hikosaka, E. Shigemasa, F. Penent, P. Lablanquie, T. Aoto and K. Ito, *Phys. Rev. A* **76**, 012717 (7 pages) (2007).

4) T. Kaneyasu, Y. Hikosaka, E. Shigemasa, P. Lablanquie, F. Penent and K. Ito, *J. Phys. B* **41**, 135101 (6 pages) (2008).

5) Y. Hikosaka, Y. Velkov, E. Shigemasa, T. Kaneyasu, Y. Tamenori, J. Liu and F. Gel’mukhanov, *Phys. Rev. Lett.* **101**, 073001 (4pages) (2008).

Micro Solid-State Photonics

Laser Research Center for Molecular Science
Division of Advanced Laser Development

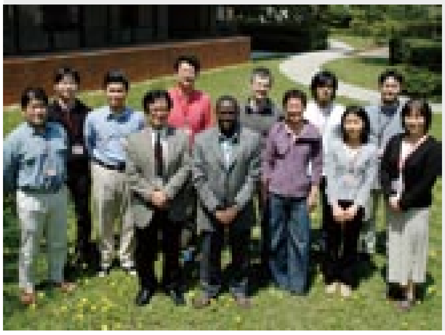

TAIRA, Takunori	Associate Professor
ISHIZUKI, Hideki	Assistant Professor
AKIYAMA, Jun	IMS Fellow
TSUNEKANE, Masaki	Post-Doctoral Fellow*
SATO, Yoichi	Post-Doctoral Fellow
SAIKAWA, Jiro	Post-Doctoral Fellow†
OISHI, Yu	Post-Doctoral Fellow‡
ONO, Yoko	Secretary
INAGAKI, Yayoi	Secretary
SUZUKI, Yukie	Secretary (for ASSP 2008 conference)

The artistic optical devices should be compact, reliable, efficient and high power light sources. With the approaches of domain structures and boundaries engineering, it is possible to bring the new interaction in their coherent radiation. The high-brightness nature of Yb or Nd doped single crystal or ceramic microchip lasers can realize efficient nonlinear wavelength conversion. In addition, designed nonlinear polarization under coherent length level allows us new function, such as the quasi phase matching (QPM). The development of "***Micro Solid-State Photonics***," which is based on the micro domain structure and boundary controlled materials, opens new horizon in the laser science.

1. High Peak Power, Passively Q-Switched Cr:YAG/Nd:YAG Micro-Laser for Ignition of Engines

The diode longitudinally pumped, passively Q-switched Nd:YAG/Cr:YAG micro-laser was researched and developed for ignition of automobile's engines. The length of the micro-laser module is 61 mm, comparable to that of a spark plug. The maximum output pulse energy of 2.7 mJ and totally 11 mJ was obtained at the pump duration of 500 µs (70 mJ) of QCW LDs. The pulse width was measured 0.6 ns. The M^2 value was 1.2 and longitudinal mode of the laser was single. The brightness of the micro-laser was calculated 0.3 PW/sr-cm^2. It was understood that the cross-section area of the flame kernel generated by the laser is 3-times larger than a spark plug as shown in Figure 1. The accelerated development of flame kernel due to the absence of quenching effects by electrodes shortens ignition delay and combustion time, and will improve the efficiency of real engines.

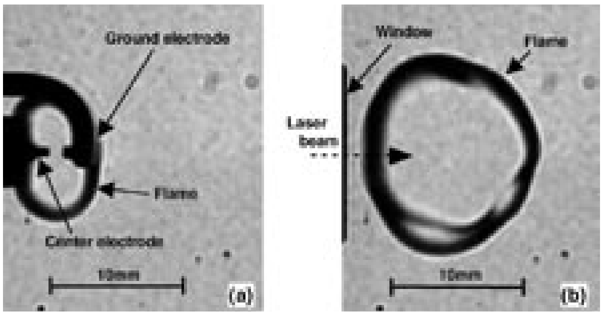

Figure 1. Schlieren photographs of the flame kernel ignited by a spark plug (a) and the micro-laser (b) in a constant volume combustion chamber at 6 ms after ignition trigger.

2. High-Energy, Broadly Tunable, Narrow-Bandwidth Mid-Infrared Optical Parametric System Pumped by Quasi-Phase-Matched Devices

We have developed a tunable, narrow-bandwidth (< 2 cm^{-1}) mid-infrared (MIR) optical parametric system with a large-aperture periodically poled Mg-doped $LiNbO_3$ (LA-PPMgLN)-based high-energy pump source. The system has a continuously tunable tuning range from 4.6 to 11.2 µm and produces a maximum output energy of 2.0 mJ at 5.1 µm as shown in Figure 2. Practical use of the MIR source is demonstrated by MIR-UV double-resonance spectroscopy of jet-cooled acetanilide.

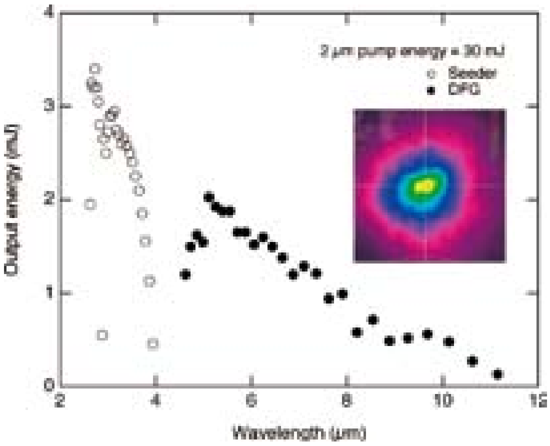

Figure 2. Tuning characteristics of the ZGP-DFG system (closed circle) and the LN-DFG system (open circle). Inset shows the intensity distribution of the ZGP-DFG system at 5.3 µm.

3. Mg-Doped Congruent $LiTaO_3$ Crystal for Large-Aperture Quasi-Phase Matching Device

We have characterized the crystal properties of Mg-doped congruent $LiTaO_3$ (MgLT), and demonstrated the first optical parametric oscillation experiment using periodically poled MgLT (PPMgLT) device. The MgLT could be a candidate for the material of high power quasi phase matching device because of the improved cut off wavelength and the decreased coercive field. The characteristics in the field poling of MgLT is similar to that of MgLN, and the coercive field of MgLT is enough low to realize a large-aperture PPMgLT device for high power applications as shown in Figure 3. We can expect the realization of several-mm-aperture PPMgLT device in near future.

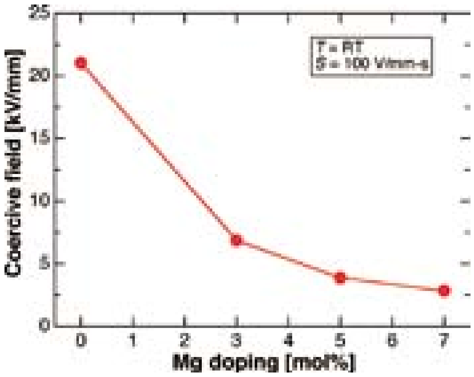

Figure 3. Coercive field of MgLT on Mg-doping (crystal temperature: T = RT, electric-field ramping rate : S = 100 V/mm-s).

4. Dependence of Rare-Earth Doped $Y_3Al_5O_{12}$ Ceramics on Doping Concentration: Electronic Structures of Host and Dopant

We have confirmed experimentally that there is severe dependence of spectral profiles of fluorescence emitted from neodymium doped $Y_3Al_5O_{12}$ (Nd:YAG) ceramics. Figure 4 shows the dependence of fluorescent spectral profile emitted from Nd:YAG on Nd^{3+}-doping concentration. It was found that there was a maximum line-shift of 2 cm^{-1} in fluorescence peaks from 1.0 at.% to 8.9 at.% Nd^{3+}-concentration (C_{Nd}). Maximum line broadening of 1.85 times was also detected due to heavily Nd^{3+}-doping. It directly indicates that heavily Nd^{3+}-doping makes the peaks of stimulated emission cross section.

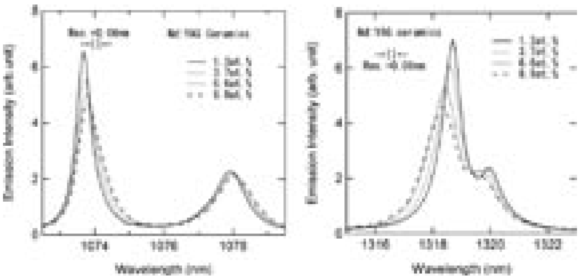

Figure 4. The dependence of fluorescent spectral profile emitted from Nd:YAG on Nd^{3+}-doping concentration. Heavily doping concentration causes both line shift and spectral-broadening.

References

1) M. Tsunekane, T. Inohara, A. Ando, K. Kanehara and T. Taira, *Tech. Digest of Advanced Solid State Photonics (ASSP2008)*, MB4 (2008).

2) J. Saikawa, M. Miyazaki, M. Fujii, H. Ishizuki and T. Taira, *Opt. Lett.* **33**, 1699–1701 (2008).

3) H. Ishizuki and T. Taira, *Tech. Digest of Conf. on Lasers and Electro-Optics (CLEO2008)*, CWG1 (2008).

4) Y. Sato, J. Akiyama, T. Taira and A. Ikesue, *Tech. Digest of The 15th International Conference on Luminescence and Optical Spectroscopy of Condensed Matter (ICL'08)* Tu-P-62 (2008).

---

* from JST Innovation Plaza Tokai

† from Tokyo Institute of Technology

‡ from RIKEN

Photo-Induced Dynamics and Reactions at Solid Surfaces

Laser Research Center for Molecular Science
Division of Ultrahigh Resolution Optical Measurement

MATSUMOTO, Yoshiyasu Professor*
WATANABE, Kazuya Assistant Professor*

Solid surfaces provide an interesting environment where two completely different electronic systems meet to each other: Localized electronic system, *i.e.*, atoms and molecules and delocalized one, *i.e.*, solid bulk surfaces. Charge transfer at surfaces is fundamental to adsorbate-metal interactions and reactions. Moreover, dynamic processes including chemical reactions on surfaces, particularly metal surfaces, are associated with continuous nonadiabatic transitions. This research program aims for understanding electron and nuclear dynamics at surfaces. Photo-induced processes including photochemistry at surfaces are the major focus in this program. Photons are used for not only exciting electronic states of adsorbate and substrate, but also for probing those states with various types of nonlinear optical spectroscopy.

1. Ultrafast Dynamics at Well-Defined Surfaces[1)]

To understand the mechanism of surface photochemistry, it is vital to know how photoinduced electronic excitation induces adsorbate nuclear motions that ultimately lead to chemical reactions. We have demonstrated the real-time observations of surface phonons and adsorbate-substrate vibrational modes by fs time-resolved second harmonics generation (TRSHG). If an excitation light pulse has a duration sufficiently shorter than a period of a vibrational mode or a phonon mode, it can excite the mode with a high degree of temporal and spatial coherence. This coherent nuclear motion modulates the second-order susceptibility $\chi^{(2)}$. Thus, by monitoring the intensity modulation of the second harmonics (SH) generation of a probe pulse, we can observe the evolution of the coherent nuclear motion subsequent to the electronic excitation at the surfaces. We have focused on the excitation mechanism of coherent surface phonons at Na-covered Cu(111) surfaces.

Changing the photon energy of the pump pulse (25 fs) from 2.0 to 2.5 eV, the oscillation amplitude derived from the Na–Cu stretching motion is enhanced. As shown in Figure 1, the careful measurements of photon-energy dependence indicates that the excitation efficiency mimics the absorbance of bulk Cu. Holes created in the d-bands by the optical transitions could be filled by electrons in the adsorbate-induced occupied state of the metallic quantum well by an Auger-type transition. Hence, holes can be created in the adsorbate-induced occupied state. Moreover, since this Auger decay can occur significantly faster than the oscillation period of the Na–Cu stretching mode, the substrate excitation may be a possible excitation mechanism for the coherent oscillation.

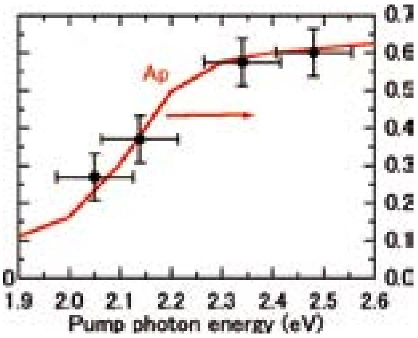

Figure 1. Action spectrum for the initial amplitude of the oscillating component in TRSHG traces due to the coherent Na–Cu stretching mode.

2. Spectroscopy of Molecules at Interfaces in Organic Field Effect Transistors by a Sum Frequency Generation Microscope

Organic field effect transistors have gained substantial attentions recently. In order to understand the efficiency of the device and the mechanism of charge transport, it is important to know carriers at the interface between a gate electrode and an organic semiconductor thin film. Since the interface is buried in the device, there are a few methods to investigate what is really happening at the interface. Sum frequency generation (SFG) is one of promising methods to realize it, since this is sensitive to the molecules at interfaces. SFG is a nonlinear optical process and, in particular, when visible and infrared beams are used, SFG is a powerful means for vibrational spectroscopy. We have developed a SFG microscope and applied it to the interface between pentacene and silicon oxide at the gate electrode. SFG signals generated at the interface are spatially resolved by the SFG microscope. We found that SFG signals are largely enhanced when carriers are injected at the interface.

3. Chemistry of One-Dimensional Nano-Surface Compounds

The fluctuating configurations of low-dimensional structures can be thermodynamically favorable at finite temperatures, because the energy gain overcomes the energy cost that accompanies local structural fluctuation. In particular, one-dimensional (1D) systems have a propensity to be sensitive to these fluctuations as described by one of the maxims of condensed matter physics, *i.e.*, one chain does not make a crystal. Thus, the dynamical formation of active species and sites by these fluctuations is a key factor in establishing a microscopic model for chemical reactions at surfaces and nano-structured compounds. It is well known that the adsorption of O on Ag(110) results in the formation of quasi-1D structures, AgO chains, accompanied by the mass transfer of substrate atoms.

We have studied the structures of continuous and truncated AgO chains on Ag(110) surfaces by using density functional theory (DFT) calculations. In addition, the thermal fluctuations of truncated chains are simulated by using the Monte Carlo method. Although it is known that oxygen elimination by CO from one dimensional AgO chains takes place exclusively at chain ends when the chains keep a linear structure at low temperatures, the structure of chain ends has been unexplored. The DFT calculations reveal that oxygen-terminated chains are more stable than silver-terminated ones and have an enhanced density of states near the Fermi level at the terminal oxygen, which is consistent with scanning-tunneling microscope (STM) observations. The Monte Carlo simulations with pairwise interactions between AgO units reproduce characteristic features observed in STM studies, including the existence of an onset temperature for the chain fluctuations and the oxygen-coverage dependence of average chain length. The onset temperature, on the one hand, is largely controlled by attractive interactions in the direction parallel to chain growth. On the other hand, the spatial distribution of fragmented AgO chains depends strongly on repulsive interactions in the direction perpendicular to chains. In particular, the repulsive interactions ranging ten units of the lattice constant in the direction perpendicular to the AgO chains are essential to mimic STM observations, where fragmented chains almost keep the mutual distance inherent to the (n×1)-O phase even under thermal fluctuations.

Reference

1) M. Fuyuki, K. Watanabe, D. Ino, H. Petek and Y. Matsumoto, *Phys. Rev. B* **76**, 115427 (5 pages) (2007).

---

* Present Address; Kyoto University, Graduate School of Sciences, Department of Chemistry, Kyoto 606-8502

Visiting Professors

Visiting Professor

MIDORIKAWA, Katsumi *(from RIKEN)*

XUV Nonlinear Optics and Attosecond Dynamics in Atoms and Molecules

Nonlinear optical process in the XUV region is of paramount importance not only in the field of quantum electronic but also in ultrafast optics. From the viewpoint of quantum electronics, new features of the interaction between intense XUV photons and matters are expected to be revealed through observation of those nonlinear phenomena. On the other hand, those nonlinear processes in the XUV region is indispensable for progress of attosecond science including attosecond atomic/molecular physics and chemistry, because it is very useful for investigating ultrafast phenomena directly in attosecond time scale. Using high harmonic generation by intense femtosecond lasers, we are pursuing extreme optical science including XUV nonlinear optics and attosecond physics/chemistry.

Visiting Professor

TOMINAGA, Keisuke *(from Kobe University)*

Molecular Dynamics in Condensed Phases Studied by Ultrafast Laser Spectroscopy

Molecules in liquids interact with each other in a complex manner, and this complicated interaction is a source of various aspects of the dynamical behaviors in liquids. Mainly, we employ two ultrafast spectroscopic techniques. One is terahertz time-domain spectroscopy. We have studied collective dynamics of liquid methanol from analysis of THz spectra based on the results by molecular dynamics simulation. The other technique is infrared nonlinear spectroscopy such as three-pulse photon echo. By this method we have made data base of time correlation functions of the frequency fluctuation of vibrational transitions of various solute/solvent systems.

Visiting Associate Professor

OKADA, Kazumasa *(from Hiroshima University)*

Study on the Fragmentation of Molecules and Clusters in the Inner-Valence and Inner-Shell Electron Excitation Regions

The knowledge of the mechanisms involved in the ionization helps us to understand various processes in which there exists interaction of molecules and photons or electrons. The fragmentation dynamics of highly-excited or multiply-ionized molecules and clusters is studied by means of time-of-flight mass spectrometry. Multiple modes of measurement are used to obtain branching ratios of fragment ions or breakdown diagrams. Kinetic energy distribution of fragments provides insight into the nature of the fragmentation process.

Visiting Associate Professor

AMEMIYA, Kenta *(from High Energy Accelerator Research Organization)*

Development of Soft X-Ray Optics and X-Ray Absorption Techniques

The soft X-ray region includes absorption edges of light elements such as carbon, nitrogen and oxygen, which are main components of organic molecules. X-ray absorption spectroscopy (XAS) is a powerful technique to investigate atomic and electronic structures of condensed materials, owing to its element and orbital selectivity. Soft X-rays with high energy resolution is necessary, however, in order to obtain significant information from X-ray absorption spectra. We develop a high-resolution soft X-ray beamline in UVSOR, as well as a novel experimental technique, three-dimensional XAS, which combines soft X-ray microbeam with the depth-resolved XAS technique. By applying this technique, lateral and depth profiles of atomic and electronic structures of organic thin films can be determined with lateral and depth resolution of several micron and sub nanometer, respectively.